Effects of interfacial roughness on phonon transport in bilayer silicon thin films

Weiyu Chen,[1] Juekuan Yang,[1,*] Zhiyong Wei,[1] Chenhan Liu,[1] Kedong Bi,[1] Dongyan Xu,[2] Deyu Li,[3] and Yunfei Chen[1,†]

[1]*School of Mechanical Engineering and Jiangsu Key Laboratory for Design and Manufacture of Micro-Nano Biomedical Instruments, Southeast University, Nanjing, 210096, People's Republic of China*

[2]*Department of Mechanical and Automation Engineering, The Chinese University of Hong Kong, Shatin, N.T., Hong Kong SAR, People's Republic of China*

[3]*Department of Mechanical Engineering, Vanderbilt University, Nashville, Tennessee 37235, USA*

We report on molecular dynamics studies of phonon (lattice vibrations) transport in bilayer silicon thin films stuck together via van der Waals interactions. Results indicate that for bilayer thin films with an atomically smooth interface, the in-plane thermal conductivity of the bilayer films is the same as that of a single layer; however, the in-plane thermal conductivity of bilayer films is higher than that of single films if roughness is introduced at the interface. These observations are explained by the effects of interfacial roughness on phonon specularity parameters for transmitted and reflected phonons.

Thermal transport through material interfaces attracts a lot of attention because of the important role it plays in thermal management of micro/nanoelectronic devices, nanostructured materials-based energy harvesting, and nanocomposites [1–5]. Recently, van der Waals (vdW) interaction mediated phonon transport at material contacts has attracted significant attention because it is commonly encountered in nanocomposites, metrology, and nanoelectronic devices [6–9]. For example, in carbon nanotubes (CNTs) and graphene based nanoelectronic devices, they are usually laid on dielectric substrates via van der Waals contacts or interfaces [10,11]. Traditionally, vdW interactions are regarded as a kind of weak coupling mechanism compared to the much stronger bonding forces such as covalent or ionic bonding. As a result, it is widely believed that phonons, the dominant energy carriers in nonmetallic nanostructures, have a high probability of being scattered at the vdW contacts, which leads to significant contact resistance [12–14]. In fact, phonon scattering at the vdW contacts has been considered to be responsible for the limited enhancement in the thermal conductivities of CNT-polymer composites [15,16].

In additional to posing resistance to thermal transport in the direction that is normal to the vdW interface, phonon behavior at vdW interfaces could also have important effects to energy flow in the direction parallel to the vdW interface. For example, it has been shown that the in-plane thermal conductivity of multilayer graphene [17] or supported graphene [8] is lower than that of suspended single-layer graphene [17–21], which has been attributed to the interlayer phonon scattering or that between the supported graphene and the substrate [17,19–22]. On the contrary, Guo *et al.*'s [23] and Ong *et al.*'s [24] results show that the coupling force plays a positive role in the enhancement of thermal conductivity. However, the underlying mechanism behind these phenomena is the change of phonon dispersion in the components of the coupling systems. These components usually have low dimensional structures, such as atom chains, carbon nanotubes, graphenes, etc., whose lattice vibrations are easily disturbed by the coupling strength.

While interlayer vdW interactions affect the in-plane phonon transport in coupling systems through changing the phonon dispersion, another different mechanism has been found recently. Yang *et al.* [6] demonstrate experimentally that the in-plane thermal conductivity of a bilayer boron nanoribbon stuck together through vdW forces could be significantly higher than that of a single boron nanoribbon, which is explained as follows. The low frequency phonons responsible for thermal transport in these boron nanoribbons have a much longer bulk mean free path than the film thickness. As such, in a single nanoribbon, the effective phonon mean free path is dominated by the film thickness due to the strong phonon-boundary scattering. A clean vdW interface between two identical ribbons, however, allows for a significant portion of phonons to transmit through ballistically without being scattered, which extends the effective phonon mean path and leads to an enhanced thermal conductivity.

One issue that is not explicitly discussed in Yang *et al.*'s report is the specularity parameter at the vdW interface, even though it is assumed in their discussion that the specularity parameters for the reflected phonons from the free surfaces of the suspended ribbons and the vdW interfaces are identical. However, for double ribbons to have an enhanced in-plane thermal conductivity, the transmitted phonons have to have a much higher specularity parameter than reflected phonons. In fact, in their discussion the specularity parameter for transmitted phonons are assumed to be unity by regarding phonon transmission as ballistic. As such, the specularity parameters for transmitted and reflected phonons at the vdW interface take very different values.

Given the importance of roughness in determining the specularity parameters, here we report on studies using nonequilibrium molecular dynamics (NEMD) simulation to assess the effects of roughness at vdW interfaces on in-plane thermal conductivity of single and bilayer silicon thin films. Our results indicate that roughness does play a critical role and determine whether the in-plane thermal conductivity is enhanced for bilayer thin films.

Figure 1(a) shows the schematic of the simulation domain composed of two layers of silicon thin films sticking together via a vdW interface. Periodic boundary conditions are applied

―――――――
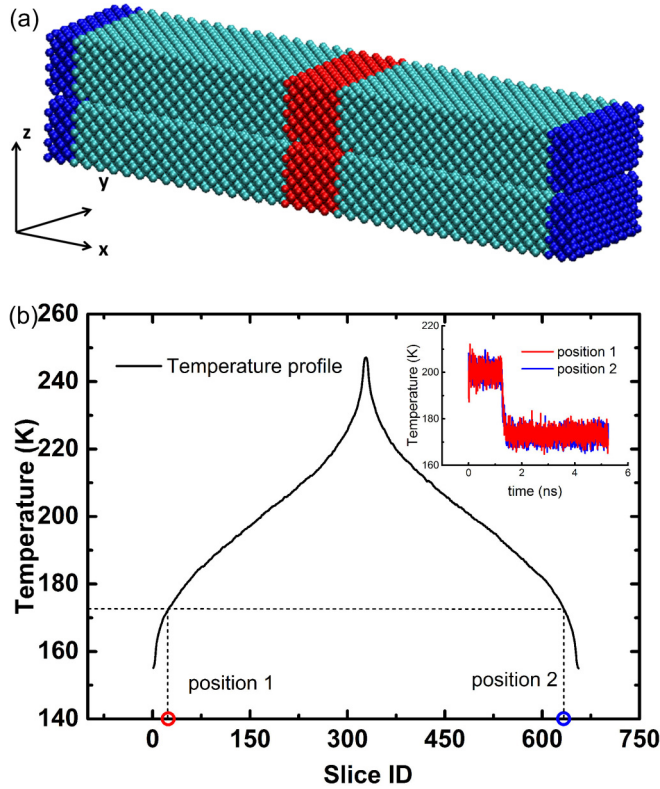*yangjk@seu.edu.cn
†yunfeichen@seu.edu.cn

FIG. 1. (Color online) (a) Schematic of the simulation domain. Periodic boundary conditions are applied in both x and y directions, and free boundary condition is used in the z direction. Heat source (red region) is located at the center of the simulation cell, while heat sink is located at the edges (blue region). The heat flux is imposed along the x direction. (b) Typical temperature profile along the heat flux direction. The inset is the temperature variation with the simulation time at position 1 and 2.

in both x and y directions with free boundaries at the top and bottom surfaces in the z direction. As such, any stress along the z direction can be released. The lattice constant is set as the equilibrium lattice constant at the simulation temperature, which is extracted by running a separate simulation of bulk silicon crystal using an NPT ensemble, which indicates that the lattice constant varies approximately linearly with temperature. It is worth noting that even though there is a temperature gradient along the heat flux direction, the stress along the x direction should still be minimal considering the almost linear dependence of the lattice constant on the simulation temperature. In the simulation, a heat source (red region) is imposed at the center of the simulation domain, while heat sinks are located at the two ends of the simulation domain (blue regions). This configuration produces a bilateral symmetric temperature profile about the heat source, as shown in Fig. 1(b).

We use the molecular dynamics package LAMMPS [25,26] with the Stillinger-Weber [27] potential for interactions between silicon atoms in each silicon layer. The interaction between silicon atoms in different silicon layers is modeled with the Lennard-Jones (LJ) potential to represent the vdW interface between the two films [28]. The LJ potential is

expressed as

$$V(r) = C_{LJ}4\varepsilon\left[\left(\frac{\sigma}{r}\right)^{12} - \left(\frac{\sigma}{r}\right)^{6}\right]. \qquad (1)$$

The parameter C_{LJ} is set as either 0 or 1. With $C_{LJ} = 0$, the two silicon thin films do not interact with each other, which represents two freestanding films. On the other hand, for $C_{LJ} = 1$, the two films are coupled together through the vdW interaction. For all calculations we have $\varepsilon = 0.01344\,\text{eV}$ and $\sigma = 0.384\,\text{nm}$, which is adopted from Ref. [28]. In all simulations, the time step is set as 0.5 fs and the whole system is first equilibrated under an NVT ensemble for 1 ns, which is followed by a 0.25 ns process under an NVE ensemble to check whether the simulation temperature is stable at the set value. After confirming that the system reaches equilibrium, a heat flux is imposed by adding energy ΔE per unit time to the heat source and subtracting an equal amount of energy from the heat sink at the same time. The heat flux q is obtained by

$$q = 0.5 \cdot \Delta E / A, \qquad (2)$$

where A is the cross-sectional area normal to the heat flux direction. The factor of 0.5 is used in formula (2) due to the period boundary condition applied along the x direction, leading to two paths for heat energy transport from the heat source to the heat sink. With the heat flux imposed, another 1 ns simulation is performed for the system to reach steady state, after which the temperature profile is extracted from the average of over 3 ns additional simulation. Based on the imposed heat flux and the obtained temperature profile, we can derive thermal conductivity using the Fourier's law

$$q = -k\frac{dT}{dx}, \qquad (3)$$

where k is the thermal conductivity, and dT/dx is the temperature gradient along the heat flux direction.

The in-plane thermal conductivities of bilayer silicon thin films of different lengths (half of the simulation domain length) ranging from 20 to 120 nm at a simulation temperature of 200 K are calculated from Eq. (3), as shown in Fig. 2. The uncertainty of the thermal conductivity is estimated by considering the uncertainty of the temperature gradient. We set the simulation temperature to 200 K to observe the phenomena with less interference from Umklapp scattering. When C_{LJ} is set as 0, the two thin films do not interact with each other, in which case the calculated thermal conductivity should equal to that of a single layer thin film. On the other hand, if C_{LJ} is set to 1, a vdW interface is formed between the two contacting thin films. According to Yang *et al.*'s explanation of their experimental observation, a portion of phonons striking the vdW interface will transmit through ballistically, which significantly extends the effective phonon mean free path, leading to an enhancement to the in-plane thermal conductivity for bi-layer thin films.

However, the simulation results shown in Fig. 2 do not follow the experimental trend, i.e., no thermal conductivity enhancement is observed for bilayer thin films. To understand this difference between experimental and numerical results, it is necessary to examine the detailed behavior of phonons when they hit the interface. When a phonon strikes an interface, it can be specularly reflected, diffusely scattered, or ballistically
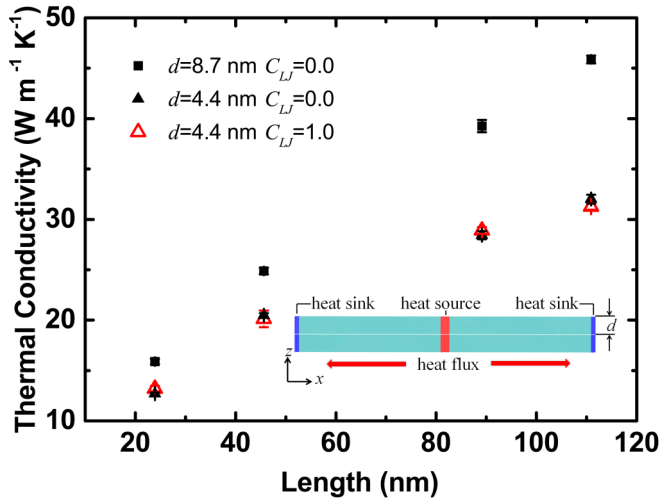
FIG. 2. (Color online) The in-plane thermal conductivity of bi-layer silicon thin film with perfect surface at 200 K as a function of the film lengths (ranging from 20 to 120 nm). The black square and triangle symbols represent the thickness dependent thermal conductivity of the bilayer silicon thin film without vdW interaction, while the red hollow triangle stands for that with vdW interaction.

FIG. 3. (Color online) The in-plane thermal conductivity of bi-layer silicon thin film with rough surface at 200 K as a function of the film lengths (ranging from 20 to 120 nm). The black triangle symbols represent the thermal conductivity of the bilayer silicon thin film without vdW interaction, while the red hollow triangle stands for that with vdW interaction.

transmitted through. One difference between the experimental case and the numerical model is that for the boron nanoribbons in the experimental studies, a surface amorphous layer of 0.5–1 nm exists, which leads to surface roughness. This surface roughness, even though extremely small, is significant enough to render the reflected phonons of a very small specularity parameter. According to Ziman, the specularity parameter for reflected phonons can be expressed as [29]

$$p = \exp\left(\frac{-16\pi^3\eta^2}{\lambda^2}\right), \tag{4}$$

where η is the asperity parameter and λ is the wavelength of incident phonons. For any phonons with a wavelength smaller than 10 nm, Eq. (4) gives a specularity parameter that is lower than 1% with a roughness of mere 1 nm. As such, for the experimental case, we can regard the reflected phonons from the interface as diffusely scattered, and if the transmitted phonons are ballistic, then the effective phonon mean free path will be extended significantly, leading to the observed enhancement in the in-plane thermal conductivity. However, for the numerical model, since the interface is atomically flat, a significant portion of the reflected phonons will be specular. In this case, the condition for thermal conductivity enhancement becomes that the specularly reflected phonons plus the ballistically transmitted phonons in the bilayer film should exceed the total specularly reflected phonons in a single freestanding film. Unfortunately, the data shown in Fig. 2 suggest that this condition is not satisfied. Instead, the simulation results indicate that the percentage of phonons that retain their in-plane momentum when they strike the vdW interface in the bilayer case or a free surface in the single ribbon case are approximately the same. The significant difference between the experimental observation and the MD simulation suggests that surface roughness plays a critical role in the in-plane thermal conductivity of bilayer thin films.
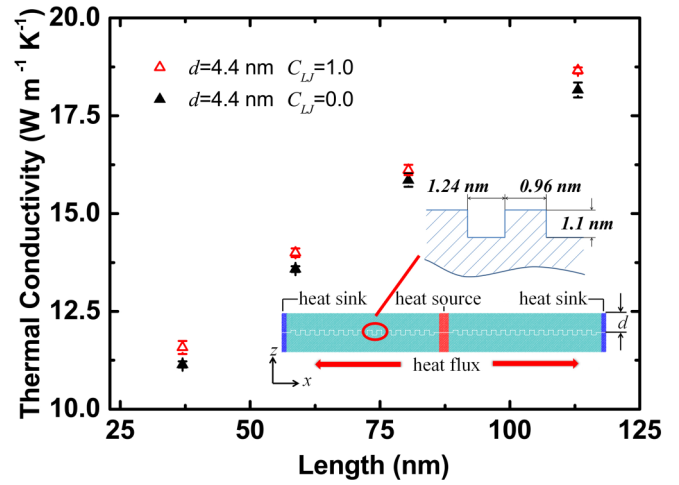
It is worth noting that the calculated in-plane thermal conductivity of the 4.4 nm thick single layer thin films from the MD simulation is much higher than what would be expected based on diffuse boundary scattering, which indicates that the specularity parameter of the free surfaces has to be significant. Therefore, to replicate the experimental trend where phonons are diffusely scattered at the ribbon surface, we seek to introduce roughness to the boundary. In this study, we introduce periodic roughness on the vdW interface into the bilayer film to reduce the specularity parameter for each single film as shown in the inset of Fig. 3. The height of the roughness is set as 1.1 nm and the widths of peak and valley are set as 0.9625 and 1.2375 nm, respectively. These parameters are chosen to keep a proper x-component distance between the upper peak and the lower peak to avoid extra repulsive force between the peaks from the two sides of the interface. For simplicity, this roughness is not applied on the top and bottom side of the bilayer thin films.

Figure 3 shows the thermal conductivities of bilayer silicon thin films corresponding to both $C_{LJ} = 0$ and $C_{LJ} = 1$. First, the thermal conductivity values for both the bilayer and single layer films are lower than those in Fig. 2, indicating that the introduced roughness does help to induce more diffuse scattering at the boundaries. Interestingly, introducing the interfacial roughness does lead to higher thermal conductivities for bilayer thin films than those of single freestanding thin films. Note that even though the enhancement is not as significant as the experimental case, it is beyond the numerical uncertainty. Comparison of the results in Figs. 2 and 3 strongly suggests that the difference is indeed due to the roughness at the interface. As such, these data verify that interfacial roughness helps to reduce the specularity of reflected phonons, leading to lower thermal conductivity of single freestanding thin films. For bilayer films, however, a portion of phonons transmit through the vdW interface ballistically, which helps to increase the overall specularity parameter of the vdW interface

and renders an effective phonon mean free path longer than that in a single freestanding film, which leads to an enhanced thermal conductivity as compared with corresponding single layer films.

In order to further confirm that the introduced roughness does reduce the phonon specularity parameter, we use NEMD to model two additional cases with different roughness patterns. The phonon specularity parameter for each case is then extracted through a kinetic model based on the Boltzmann transport equation. Figure 4(a) is the schematic of the new simulation domain with periodic boundary conditions applied only along the y direction. The heat source (red region) and heat sink (blue region) are located at the two ends of the model. Two unit cells at the two ends are fixed during the simulation. We adopt this new approach to make full use of the simulation domain length. The simulation was conducted the same as previously described except that the temperature is set at 300 K for the convenience of theoretical fitting using the Boltzmann transport equation (BTE). The top and bottom surfaces are employed with periodic rectangular roughness. The height of the roughness is set as 0.55 nm and the widths of the peak and valley are set the same for all cases and w is the periodic length of the roughness. The boundaries are perfectly smooth when w is set to infinity. Figure 4(b) plots the thermal conductivity calculated using the distance between the peaks from the top side and the bottom side as the film thickness, depicted as d_1 in Fig. 4(a). Figure 4(c) presents the thermal conductivity with the film thickness taken as the distance between valleys, depicted as d_2 in Fig. 4(a). For the thin film with perfectly smooth boundaries, there is no peaks or valleys. In this case, thermal conductivity is calculated using the distance between the top side and the bottom side as the film thickness, depicted as d. Both Figs. 4(b) and 4(c) show that the thermal conductivity decreases as surface roughness is introduced. The theoretical results using the kinetic model [30] with different specularity parameters are also shown in the figure as solid lines. To compare with the results from the kinetic model, the scatter values in Figs. 4(b) and 4(c) are reduced MD thermal conductivity after quantum correction [31]. According to this model, the thermal conductivity of thin films is written as [30]

$$k_{\text{film}} = \frac{3k_B \omega_D}{4\pi c} \frac{1}{N} \sum_{i=1}^{N} g(\omega_i, \theta_i, \phi_i, \xi_i), \qquad (5)$$

where k_B is the Boltzmann constant, $\omega_D = c(6\pi^2/\Omega)^{1/3}$ is the Debye frequency, and $c = 2737$ m/s is the speed of sound averaged between the three acoustic branches, two transverse and one longitudinal mode [30]. Ω is the primitive cell volume. For silicon with a diamond structure, the primitive cell volume is $a^3/4$, where $a = 0.543$ nm is the lattice constant. θ and φ are the spherical angles, ξ is a random number ranging from 0 to 1, N is the sampling number. $g(\omega, \theta, \varphi, \xi)$ is the integral function, which is expressed as

$$g(\omega, \theta, \phi, \xi) = \frac{(\hbar\omega/k_B T)^2 e^{\hbar\omega/k_B T}}{(e^{\hbar\omega/k_B T} - 1)^2} \omega^2 \tau(\omega, \theta, \phi, \xi) \cos^2\theta \sin\theta, \qquad (6)$$

where $\hbar$ is the reduced Planck constant, and $T = 242$ K (after quantum correction) is the temperature. τ is the averaged phonon relaxation time. Matthiessen's rule is applied to
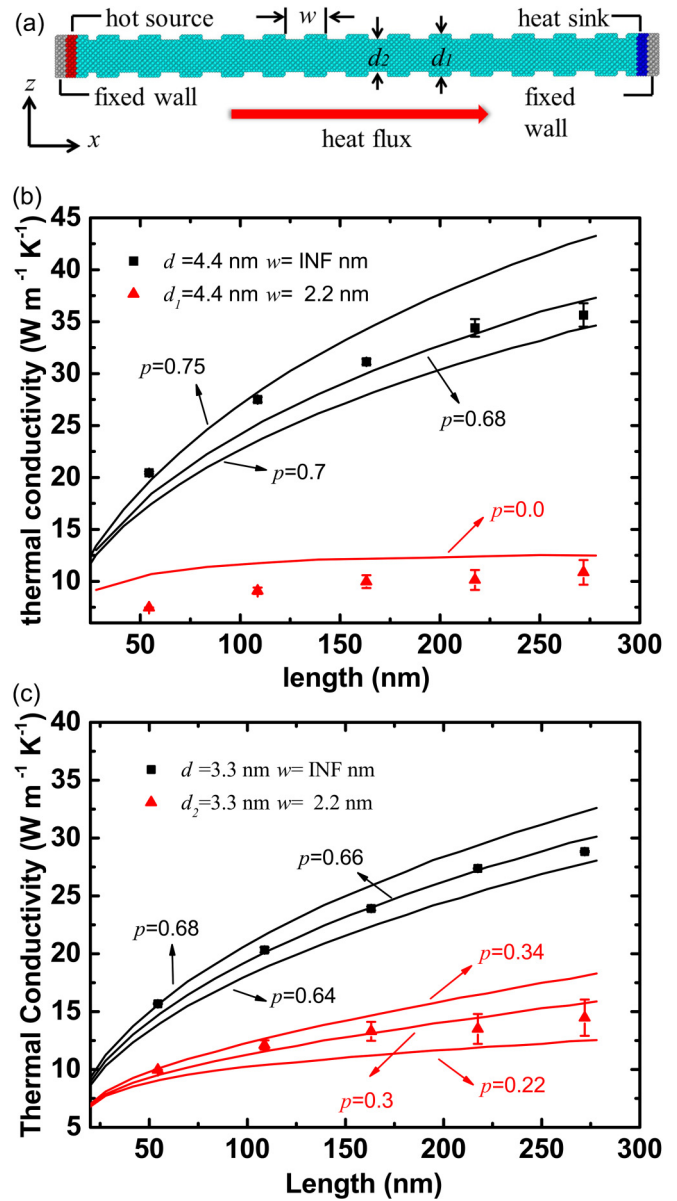

FIG. 4. (Color online) (a) The schematic of the simulation model. Periodic boundary conditions are applied in y direction, and free boundary condition is used in the z direction. Heat source (red region) is located at the center of the simulation cell, while heat sink is located at the edges (blue region). The heat flux is imposed along the x direction. Two unit cells at the most two ends are fixed during the simulation procedure. The in-plane thermal conductivity of single layer silicon thin film with different rough surfaces at 300 K (after quantum correct is 242 K) as a function of the film lengths (ranging from 50 to 300 nm). The scatters are NEMD simulation results after quantum correction and the curves are obtained by fitting the BTE with a kinetic model. Thermal conductivities are calculated using d_1(b) or d_2(c) as the film thickness.

combine the effects of phonon-phonon (τ_∞) and phonon-boundary (τ_B) scattering, which yields

$$\tau(\omega, \theta, \phi, \xi) = \frac{\tau_\infty(\omega)\tau_B(\theta, \phi, \xi)}{\tau_\infty(\omega) + \tau_B(\theta, \phi, \xi)}. \qquad (7)$$

τ_∞ is modeled using a relationship proposed by Callaway [32]. $\tau_\infty = 1/(A\omega^2)$, where $A = 4.12 \times 10^{-17}$ is a temperature dependent parameter which can be fitted with the thermal conductivity of bulk silicon k_{bulk} at the temperature T as follows:

$$A(T) = \frac{k_B}{2\pi^2 c k_{\text{bulk}}} \int_0^{\omega_D} \frac{(\hbar\omega/k_B T)^2 e^{\hbar\omega/k_B T}}{(e^{\hbar\omega/k_B T} - 1)^2} d\omega. \quad (8)$$

τ_B is expressed as [30]

$$\tau_B(\theta,\phi,\xi) = \begin{cases} l_l/c & \text{if} \quad l_l < l_e \text{ and } \xi > p, \\ l_e/c & \text{otherwise,} \end{cases} \quad (9)$$

where p is the specularity parameter, which is used as the fitting variable here. l_e is the averaged distance traveled ballistically by a phonon before hitting the end boundary, and l_l is the averaged distance traveled ballistically by a phonon before hitting the lateral boundary. l_e and l_l are given as [33]

$$l_e(\theta,\phi) = \frac{L}{2|\cos\theta|} \quad \text{and} \quad l_l(\theta,\phi) = \frac{d}{2|\cos\phi\sin\theta|}, \quad (10)$$

where L and d are the length and thickness of the thin film to be modeled, respectively. By randomly choosing the values of ω, θ, φ, and ξ in the range of $[0, \omega_D]$, $[0,\pi]$, $[0,2\pi]$, and $[0,1]$ respectively, thermal conductivity of thin films with length L and thickness d can be calculated through Eqs. (5)–(10). Figure 4(b) shows that the red triangle values are even below the lowest fitting curve yielded from the kinetic model by setting $p = 0$. This is because the maximum thickness d_1 is used as the film nominal thickness in calculating the thermal conductivity for the rough film. In Fig. 4(c), d_2 is used as the film nominal thickness. The results demonstrate that the surface roughness can reduce the phonon specularity parameter effectively from 0.66 to less than 0.3, which clearly demonstrate the effectiveness of introducing roughness to the vdW interface to enhance the diffuse scattering for incident phonons.

In summary, we simulate the in-plane thermal conductivity of single and bilayer silicon thin films with perfectly smooth and rough interfaces between the constituent single layer films using the NEMD method. For smooth interface, our results show that due to a relatively high specularity parameter, the thermal conductivity of bilayer thin films is almost the same as that of single layer films. In the case of a vdW interface with roughness, the specularity parameter for the reflected phonons is significantly reduced while transmitted phonons maintain a high specularity parameter, which leads to extended effective phonon mean free path and an enhanced thermal conductivity, as that observed experimentally with boron nanoribbons.

[1] G. Chen and A. Shakouri, Heat transfer in nanostructures for solid-state energy conversion, J. Heat Transfer **124**, 242 (2002).

[2] D. G. Cahill, W. K. Ford, K. E. Goodson, G. D. Mahan, A. Majumdar, H. J. Maris, R. Merlin, and S. R. Phillpot, Nanoscale thermal transport, J. Appl. Phys. **93**, 793 (2003).

[3] O. Breuer and U. Sundararaj, Big returns from small fibers: A review of polymer/carbon nanotube composites, Polymer Composites **25**, 630 (2004).

[4] A. A. Balandin, Thermal properties of graphene and nanostructured carbon materials, Nat. Mater. **10**, 569 (2011).

[5] D. G. Cahill *et al.*, Nanoscale thermal transport. II. 2003–2012, Appl. Phys. Rev. **1**, 011305 (2014).

[6] J. Yang *et al.*, Enhanced and switchable nanoscale thermal conduction due to van der Waals interfaces, Nat. Nanotechnol. **7**, 91 (2012).

[7] R. Prasher, Acoustic mismatch model for thermal contact resistance of van der Waals contacts, Appl. Phys. Lett. **94**, 041905 (2009).

[8] J. H. Seol *et al.*, Two-dimensional phonon transport in supported graphene, Science **328**, 213 (2010).

[9] W.-P. Hsieh, A. S. Lyons, E. Pop, P. Keblinski, and D. G. Cahill, Pressure tuning of the thermal conductance of weak interfaces, Phys. Rev. B **84**, 184107 (2011).

[10] K. S. Novoselov, A. K. Geim, S. V. Morozov, D. Jiang, Y. Zhang, S. V. Dubonos, I. V. Grigorieva, and A. A. Firsov, Electric field effect in atomically thin carbon films, Science **306**, 666 (2004).

[11] R. Prasher, Graphene spreads the heat, Science **328**, 185 (2010).

[12] R. Prasher, Predicting the thermal resistance of nanosized constrictions, Nano Lett. **5**, 2155 (2005).

[13] V. Bahadur, J. Xu, Y. Liu, and T. S. Fisher, Thermal resistance of nanowire-plane interfaces, J. Heat Transfer **127**, 664 (2005).

[14] C. Dames, Pulling together to control heat flow, Nat. Nanotechnol. **7**, 82 (2012).

[15] R. S. Prasher, X. J. Hu, Y. Chalopin, N. Mingo, K. Lofgreen, S. Volz, F. Cleri, and P. Keblinski, Turning Carbon Nanotubes from Exceptional Heat Conductors into Insulators, Phys. Rev. Lett. **102**, 105901 (2009).

[16] J. K. Yang, S. Waltermire, Y. F. Chen, A. A. Zinn, T. T. Xu, and D. Y. Li, Contact thermal resistance between individual multiwall carbon nanotubes, Appl. Phys. Lett. **96**, 023109 (2010).

[17] S. Ghosh, W. Z. Bao, D. L. Nika, S. Subrina, E. P. Pokatilov, C. N. Lau, and A. A. Balandin, Dimensional crossover of thermal transport in few-layer graphene, Nat. Mater. **9**, 555 (2010).

[18] A. A. Balandin, S. Ghosh, W. Z. Bao, I. Calizo, D. Teweldebrhan, F. Miao, and C. N. Lau, Superior thermal conductivity of single-layer graphene, Nano Lett. **8**, 902 (2008).

[19] W. Cai, A. L. Moore, Y. Zhu, X. Li, S. Chen, L. Shi, and R. S. Ruoff, Thermal transport in suspended and supported monolayer graphene grown by chemical vapor deposition, Nano Lett. **10**, 1645 (2010).

[20] Z. Y. Wei, Z. H. Ni, K. D. Bi, M. H. Chen, and Y. F. Chen, In-plane lattice thermal conductivities of multilayer graphene films, Carbon **49**, 2653 (2011).

[21] D. Singh, J. Y. Murthy, and T. S. Fisher, Mechanism of thermal conductivity reduction in few-layer graphene, J. Appl. Phys. **110**, 044317 (2011).

[22] J. Chen, G. Zhang, and B. Li, Substrate coupling suppresses size dependence of thermal conductivity in supported graphene, Nanoscale **5**, 532 (2013).

[23] Z.-X. Guo, D. Zhang, and X.-G. Gong, Manipulating thermal conductivity through substrate coupling, Phys. Rev. B **84**, 075470 (2011).

[24] Z.-Y. Ong and E. Pop, Effect of substrate modes on thermal transport in supported graphene, Phys. Rev. B **84**, 075471 (2011).

[25] http://lammps.sandia.gov.

[26] S. Plimpton, Fast parallel algorithms for short-range molecular-dynamics, J. Comput. Phys. **117**, 1 (1995).

[27] F. H. Stillinger and T. A. Weber, Computer simulation of local order in condensed phases of silicon, Phys. Rev. B **31**, 5262 (1985).

[28] S. L. Mayo, B. D. Olafson, and W. A. Goddard, DREIDING: A generic force field for molecular simulations, J. Phys. Chem. **94**, 8897 (1990).

[29] J. M. Ziman, *Electrons and Phonons: The Theory of Transport Phenomena in Solids* (Clarendon, Oxford, UK, 2001).

[30] G. Xie, Y. Guo, B. Li, L. Yang, K. Zhang, M. Tang, and G. Zhang, Phonon surface scattering controlled length dependence of thermal conductivity of silicon nanowires, Phys. Chem. Chem. Phys. **15**, 14647 (2013).

[31] A. Maiti, G. D. Mahan, and S. T. Pantelides, Dynamical simulations of nonequilibrium processes - Heat flow and the Kapitza resistance across grain boundaries, Solid State Commun. **102**, 517 (1997).

[32] J. Callaway, Model for lattice thermal conductivity at low temperatures, Phys. Rev. **113**, 1046 (1959).

[33] A. J. H. McGaughey, E. S. Landry, D. P. Sellan, and C. H. Amon, Size-dependent model for thin film and nanowire thermal conductivity, Appl. Phys. Lett. **99**, 131904 (2011).